11th World Congress on Computational Mechanics (WCCM XI)
5th European Conference on Computational Mechanics (ECCM V)
6th European Conference on Computational Fluid Dynamics (ECFD VI)
E. Oñate, J. Oliver and A. Huerta (Eds)

COMPUTER SIMULATION OF FRACTURE QUASI-BRITTLE CERAMIC NANOCOMPOSITES UNDER PULSE LOADING

VLADIMIR V. SKRIPNYAK[*], EVGENIYA G. SKRIPNYAK[*], VLADIMIR A. SKRIPNYAK[*,†], IRINA K. VAGANOVA[*]

[*] Tomsk State University, Lenin av. 36, 634050, Tomsk, Russia,
skrp@ftf.tsu.ru and http://www.tsu.ru

[†] Institute of Strength Physics and Materials Sciences SB RAS, Academichisky av. 2/4, 634021
Tomsk, Russia skrp@yandex.ru and http://www.ispms.ru

Key Words: *Fracture, Heterogeneity, Probability, 3-D model, Quasi-brittle Nanocomposites, Multi-scale Simulation.*

Abstract. Multi-scale computer simulation approach has been applied to research mechanisms of failure in ceramic nanocomposites under dynamic loading. Damage nucleation and accumulation in quasi-brittle ceramics nanocomposites under impact loadings were simulated. The probability of fracture was estimated for $ZrO_2 - ZrB_2$, and $ZrO_2 - ZrB_2 - B_4C$ nanocomposites under pulse loadings of microsecond duration. The computational models of a structured representative volume (RVE) of ceramic nanocomposites were developed using the data of structure researches on meso-, micro -, and nanoscale levels. The critical fracture stress on meso-scale level depends not only on relative volumes of voids and inclusions, but also on the parameters of inclusion clusters. Damage of nano-composites can be formed under stress pulse amplitude of less than the Hugoniot elastic limit of matrix. The Hugoniot elastic limit of ceramic nanocomposites decreases with increasing the volume concentration clusters of nano-voids. The spall stress of ceramic nanocomposites depends on relative volumes and sizes of voids and inclusions. The shear strength decreasing can be caused by nano-voids near triple junctions of ceramics matrix grains and ultrafine-grained ceramics.

1 INTRODUCTION

Influence of mesoscale structure on mechanical properties of ceramic nanocomposites is investigated by experimental and computer simulation approaches [1-4]. The first challenge in ceramic nanocomposites design is to enhance the strength and fracture toughness [5]. Dynamic strength and fatigue life analysis require an understanding of mechanical behavior of nanomaterials under pulse loadings. Mechanical behavior of nanoceramics under wide range of loading conditions differs from that observed for coarse grained counterparts. A particular feature of ceramic nanocomposites is quasi-brittle fracture behavior in range of low homologous temperatures. The quasi-brittle fracture of nanocomposites is reported in [6]. For instance, particular attention is given to development of new $ZrO_2 - ZrB_2$ and $ZrO_2 - ZrB_2 - B_4C$ nanocomposites [1-2]. It should be noted, that coarse grained composites of this class exhibit brittle behavior. When developing nanocomposites on the base of boride, oxide, carbide ceramic compounds, it's assumed that new materials will exhibit the enhanced fracture toughness.

Computer simulation methods on the base of the finite element method (FEM) [7], the discrete element methods (DEM) [8], and molecular dynamics methods (MD) [9] are used for investigation on mechanical behavior of new ceramic nanocomposites. Authors of [10] proposed to use the nanostructure modeling approach for understanding the mechanical behavior of nanocomposites.

Framework of this approach contains multiscale model in which material is considered as a system of structured elements (such as grains, particles, fibers etc.) at nano-scale level and continuum media embodying averaged parameters of the mechanical state at macro-scale. Average Parameters of the mechanical state at macro-scale level are defined by homogenization in RVE. In present study, this approach was used to develop a two-scale model.

It's known, that morphological parameters of structure elements, as well as parameters of strengthening particle agglomerates and void clusters influence on mechanical properties of nanocomposites subjected to quasi-static loading conditions [5-10]. Researches on mechanical behavior of ceramic nanocomposites under dynamic loadings have not been widely presented in literature [11,12]. The aim of present study is development of a multiscale computer model of damage and fracture processes taking place in $ZrO_2 - ZrB_2$, and $ZrO_2 - B_4C$ ceramic nanocomposites under wide range of loading conditions.

2 MODEL OF MECHANICAL BEHAVIOR OF NANOCOMPOSITES.

Multi-scale computer simulation approach has been applied to research mechanisms of failure in ceramic nanocomposites subjected to dynamic loading. Response of nanocomposites to pulse loadings was estimated using results of RVE mechanical response of simulation with given phase concentrations and morphological parameters of matrix grains and strengthening inclusions. Model RVE of nanocomposites was developed using the data of micro-structural researches on some experimental specimens.

Within the present approach, computational RVE model include structure volume model. Throughout the modeling, the RVE size is established such that it contains a lower possible number of interacted structural elements of a lower-scale level providing equal values of statistically averaged physical-mechanical property parameters. It should be noted, that geometrical size of model RVE depends not only on a structure of material but also on loading conditions. This is provided by possibility that collective effect occur and result in the formation of block fragmented structure, micro-crack deflections etc. at mesoscale level. To describe the mechanical response of solid phases, the continuum approach is used. Continuum mechanics approach is appropriate for describing the deformation and damage processes on mesoscale level, if the size of structural elements l_m (grain size of matrix, grain size of reinforced particles) is greater than 50 nm. Also, size of material particles of continuum media have to satisfy the criterion of $l_m >> 50$ nm.

Characteristic sizes of RVE were set to 2.4-24 μm depending on a reinforced particles size and matrix grains size. The reinforced particles size and quantity were matched to meet a concentration condition of the RVE. In the model RVE, strengthening particles had a rectangular shape. Fig.1 shows the structured RVE and the scheme of boundary conditions corresponding to pulse loading of RVE nanocomposites.

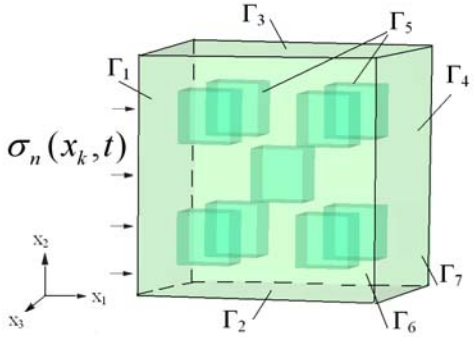

Fig.1. Meso-structure of model representative volume, boundary condition.

Mechanical state of structural elements of nanocomposites (grains of matrix, strengthening particles, grain boundaries phase) is described by meso-scale mechanical parameters.

$$\sigma_n(x_k,t)=F(x_k,t) \quad x_k \in \Gamma_1,\ k=1,2,3\ ,$$
$$u_2(x_k,t)=0,\ \ x_k \in \Gamma_2,\ x_k \in \Gamma_3.\ \ u_3(x_k,t)=0,\ \ x_k \in \Gamma_6, x_k \in \Gamma_7\ .$$
$$p=u_n[\rho C]_{\Gamma_4}\ ,\ x_k \in \Gamma_4\ .$$

Here x_k are the Cartesian coordinates, ρ is the mass density in vicinity of boundary, u_n is the normal velocity of material particle, parameter C is decreasing from longitudinal sound velocity C_l in the elastic precursor to the bulk sound velocity C_B, $F(x_k,t)$ is a function for assigning a pulse shape and duration. Contact conditions are applied on the matrix-reinforced particle boundary Γ_5.

Components of local strain rate tensor are defined by Stocks relation:

$$\dot{\varepsilon}_{ij}=\frac{1}{2}(\nabla_i u_j+\nabla_j u_i) \tag{1}$$

where $\dot{\varepsilon}_{ij}$ are components of the strain rate tensor, u_i are components of particles velocity, ∇_i is Hamilton operator, the substantial time derivative is denoted via dot notation.

Dynamics of structured RVE is described in Lagrange coordinate system by conservation equations of mass, momentum, and energy:

$$\frac{\partial\sigma_{ij}}{\partial x_j}=\rho\frac{du_i}{dt},\ \frac{d\rho}{dt}=\rho\frac{\partial u_i}{\partial x_i},\qquad \rho\frac{dE}{dt}=\sigma_{ij}\dot{\varepsilon}_{ij}\ , \tag{2}$$

where σ_{ij} are components of micro stress tensor, ρ is the mass density, u_i are components of displacement vector, ε_{ij} are components of strain rate tensor, E is the local specific internal energy per unit mass.

The strain rate tensor is expressed by sum of elastic and inelastic parts:

$$\dot{\varepsilon}_{ij}=\dot{\varepsilon}^e_{ij}+\dot{\varepsilon}^p_{ij}\ . \tag{3}$$

Components of the stress tensor are expressed by formula:

$$\sigma_{ij} = -p\delta_{ij} + S_{ij}, \tag{4}$$

where σ_{ij} are components of stress tensor, p is the pressure, S_{ij} are components of stress deviator.

Equation of state was used in polynomial form for pressures up to 10 GPa:

$$\begin{aligned} p &= K_1\theta + K_2\theta^2 + K_3\theta^3 + \Gamma\rho_0 E \quad \text{for compression } (\theta > 0), \\ p &= K_1\theta \qquad\qquad\qquad\qquad\quad \text{for tension } (\theta \le 0), \end{aligned} \tag{5}$$

where K_1, K_2, K_3 are material constants, $\theta = (\rho/\rho_0) - 1$, Γ is the Grüneisen parameter.
The nano-cracks nucleation in a condensed ceramic phase was taken into consideration.

The shear cracks nucleation reduces the shear strength of ceramic phase particles under compression. The damage parameter D is introduced to account for a decrease in the shear strength [4,13]:

$$D = \sum_{k=0} [\Delta\varepsilon^p / \varepsilon_f]_k, \tag{6}$$

where $[\Delta\varepsilon^p]_k = \int_{t_k}^{t_{k+1}} \dot{\varepsilon}^p_{eq}\, dt$, $\dot{\varepsilon}^p_{eq} = (\frac{2}{3}\dot{\varepsilon}^p_{ij}\dot{\varepsilon}^p_{ij})^{1/2}$, ε_f is strain under which fragmentation occurs.
The parameter D is equal to 0 when material is undamaged. Local failure in a point of the condensed phase occurs when D =1. The deviator effective stress tensor of damaged media is defined by relation:

$$S_{ij} = (1-D)[S_{ij}]_c, \tag{7}$$

where $[S_{ij}]_c$ are components of stress tensor of condensed phase.

Threshold of effective strain ε_f is approximated by relation [13]:

$$\varepsilon_f = D_1 (P^* + T^*)^{D_2}, \tag{9}$$

where $T^*=\sigma_{sp}/P_{HEL}$, $P^*=p/P_{HEL}$, P_{HEL} is the pressure corresponding to the Hugoniot Elastic Limit, D_1,D_2 are material constants.
Deviator stress tensor is defined using the Drucker-Prager model:

$$\frac{d[S_{ij}]_c}{dt} = 2\mu(\dot{\varepsilon}^e_{ij} - \frac{1}{3}\dot{\varepsilon}^e_{kk}\ \delta_{ij}), \frac{d[S_{ij}]_c}{dt} = [\dot{S}_{ij}]_c - [S_{ik}]_c\dot{\omega}_{jk} - [S_{jk}]_c\dot{\omega}_{ik}, \tag{10}$$

where μ is the shear modulus, $\dot{\omega}_{ik} = (1/2)(\nabla_i u_k - \nabla_k u_i)$.

$$\dot{\varepsilon}^e_{ij} = \dot{\varepsilon}_{ij} - \dot{\varepsilon}^p_{ij}, \ \dot{\varepsilon}^p_{ij} = \dot{\lambda}\ \frac{\partial g}{\partial \sigma_{ij}}, \ g = \left[\frac{1}{2}S_{ij}S_{ij}\right]^{1/2} - \sigma_s, \tag{11}$$

where σ_s is a material constant, $\dot{\varepsilon} = \dot{\varepsilon}_{eq} / 1\,[s^{-1}]$ is the normalized value of equivalent strain rate tensor, $\dot{\lambda}$ is a model parameter.

Model parameters are listed in Table 1.

Table 1: Parameters used for the computation

Parameters	ZrB_2	ZrO_2	B_4C
ρ (kg/m3)	$6.29\ 10^3$	$6.05\ 10^3$	$2.52\ 10^3$
K_1(GPa)	219.0	C33	263.0
K_2(GPa)	0	C43	480.0
K_3(GPa)	0	C53	659.0
μ(GPa)	212	76	189
Γ	1.	1.	1.
σ_{HEL}(GPa)	7.11	8.9	16.0
p_{HEL}(GPa)	3.07	5.66	7.2
σ_s(GPa)	6.07	4.86	13.2
σ_{sp}(GPa)	0.5	0.6	0.32
D_1	0.1	0.01	0.1
D_2	1.0	0.7	1

The initial conditions were used in the form

$$u_i(x_k) = u_i^{(0)},\ \sigma_{ij}(x_k) = 0,\ \rho(x_k) = \rho_{(0)}(x_k),\ \ \varepsilon_{ij}(x_k) = 0, E(x_k) = 0 \ .$$

Smooth Particle Hydrodynamics (SPH) method was used for a simulation of deformation and fracture of RVE under pulse loadings with amplitudes in the range from 5 GPa to 15 GPa [14-15].

Model of RVE containing regular nanoparticle system is shown in Fig. 2. Smoothed particles had a size of ~19,6 nm.

The concentration of phases in the volume element was set equal to specific value of concentration in macroscopic specimen. In the framework of continuum mechanics, kinematic and dynamic parameters of state are averaged over the volume of material particle.

Macro-scale kinematic parameters of structured medium can be defined using averaged components of particle velocity $< u_i >$ and components of strain rate tensor$< \dot{\varepsilon}_{ij} >$.

Particle velocities, stresses, and temperature are distributed non-uniformly over the RVE of nanocomposite. The homogenization of kinematic parameters method is appropriate for defining the displacement vector components on boundaries of the RVE:

$$< u_i > = \frac{1}{V_{RVE}} \int_0^{V_{RVE}} u_i(x_k)\, dV \quad , \tag{12}$$

where V_{RVE} is the representative volume.

Components of effective strain rate tensors and rotation rate tensor are defined by Eq. (13) and components of effective stress tensor are defined by Eq. (14):

$$< \dot{\varepsilon}_{ij} >= \frac{1}{2}[\frac{\partial < u_i >}{\partial x_j} + \frac{\partial < u_j >}{\partial x_i}],\ \dot{\omega}_{ij} = \frac{1}{2}[\frac{\partial < u_i >}{\partial x_j} - \frac{\partial < u_j >}{\partial x_i}] \quad . \tag{13}$$

where $< u_i >$ is averaged mass velocity, u_i is the local mass velocity in V_{RVE}.

$$< \varepsilon_{ij} >= \frac{1}{|V_{RVE}|}\int_0^{V_{RVE}} \varepsilon_{ij}\, dV\ , \tag{14}$$

where $< \varepsilon_{ij} >$ are the components of macroscopic strain tensor, ε_{ij} are the components of local strain tensor, V_{RVE} is the representative volume.

In this case, it's acceptable to use the continual approach for the description of inelastic strains.

The averaged mass density is defined by Eq. (15) that takes into account a distribution of phase mass densities of in RVE.

$$< \rho >= \frac{1}{|V_{RVE}|}\int_0^{V_{RVE}} \rho(x_i)\, dV\ . \tag{15}$$

Increment of specific internal energy of deformed RVE is defined in consisted with Hill-Mandel principle of macrohomogeneity as follows:

$$< \sigma_{ij} >< \dot{\varepsilon}_{ij}^{e} > = \frac{1}{|V_{RVE}|}\int_0^{V_{RVE}} \sigma_{ij}\dot{\varepsilon}_{ij}^{e}\, dV\ . \tag{14}$$

Components of the effective stress tensor can be defined by Eqs. (14).

It should be noted, that in the context of present approach, mechanical properties of multiphase medium are extracted from mechanical response so that no approximation equations predicting the properties are required.

Effective moduli of elasticity are defined by Eq. (15) using the data on computed values of longitudinal C_L and bulk C_B velocities of wave propagation.

$$< \mu >=< \rho > C_s^2\ ,\ < K >=< \rho > C_B^2\ ,\ C_L{}^2 = C_B^2 + \frac{4}{3}C_s^2\ , \tag{15}$$

where $< \rho >$ is averaged mass density in loaded part of the volume behind the front of stress wave.

3 RESULT AND DISCUSSION

Grains of crystalline phases of ceramic composites exhibit different mechanical impedances ρC_l (ρ is the mass density, and C_l is the longitudinal sound velocity). Grains of condensed phases of ceramic composites have different mechanical impedances. For ZrO_2, ZrB_2 , B_4C impedance values ρC_l are: 4.28, 5.08, 3.55 [10^7 kg/m^2 s] respectively, while the

Hugoniot adiabat curves of ZrO_2 and B_4C in the range of pressures up to 15 GPa are approximate [13,16,17,18].

On the meso-scale level, shock waves are reflected from phase boundaries. This causes strengthening particles distribution to affect a shock wave front pattern. Fig.2. shows a sequence of 3 RVE of given phase concentrations with distributed particles over the volume. Model RVE of composites and nano-composites had sizes of 24x24 μm and 2,4x2,4 μm. Sizes of strengthening particles and voids were set to 3 μm and 300 nm respectively. Fig. 2 show model RVEs with uniform distribution of particles (a) and particles clusters (b) respectively.

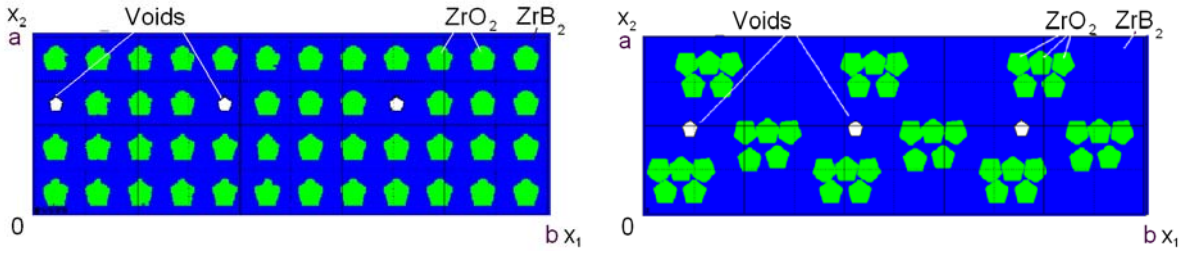

a b

Fig.2 Models of structured ceramic composites

Pressure behind the elastic wave front in RVEs shown in Fig.3.

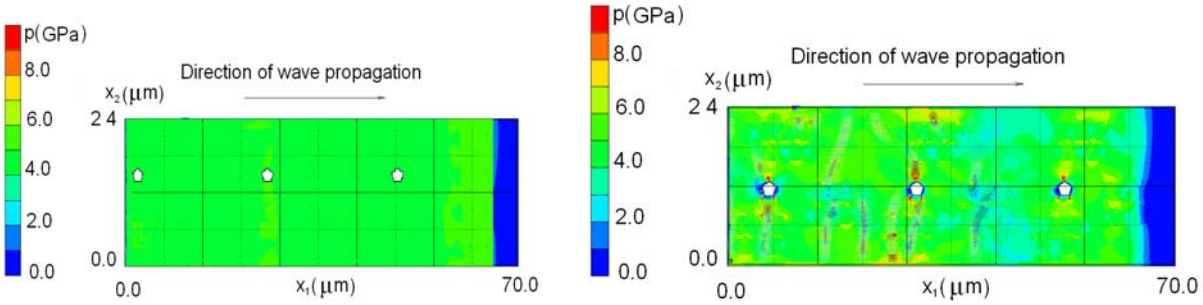

a b

Fig.3.Pressure behind the elastic stress wave in ZrB_2- 30 Vol. % ZrO_2 composite

Clusters of strengthening particles produce heterogeneous strain field behind the wave front. Difference of impedances between reinforced particle grains and the matrix cause waves to be reflected from phase boundaries and interact on meso-scale level. This effect is negligible for nanocomposites because of fine grain size. Stress pattern behind the front of elastic precursor in the RVE of uniform strengthening particle distribution is less heterogeneous than in RVE with clusters. On the meso-scale level, occurring stress gradients may cause a local microcrack nucleation. A possibility of crack nucleation depends not only on shear and tensile stress thresholds but also on time criterion of crack nucleation and growth at micro-scale level. To evaluate time required for microcrack nucleation in condensed phase, the S.N. Zhurkov formula can be used:

$$\tau(\sigma,T)=\tau_0 \exp(\frac{U_0-\gamma\sigma}{kT}), \qquad (16)$$

where τ is a fracture life, $\tau_0 \approx 10^{-13}$ s , k is the Boltzmann constant, U_0 is the dissociation

energy of matter, T is the temperature, $\gamma = qV_a$, V_a is the activation volume, q is the stress concentration parameter near defects.

The dissociation energy U_0 of ZrB_2, ZrO_2, B_4C can be varied in ranges of 2482 −2540, 700−820, 1350 −2030 kJ/kg respectively [19]. Therefore, microcrack nucleation times for condensed ZrB_2, ZrO_2, B_4C matrix are on the order of 10^{-10} s, 10^{-9} and 10^{-8} s^{-1} respectively. These microcrack nucleation times were in agreement with these obtained from the simulation. The presence of nano-particles clusters in the RVEs may cause local strain heterogeneity. Relaxation of local shear stress heterogeneity is associated with nanocracks nucleation. Shear bands do not grow in a compression wave. Growth of microcraks and micro-cavity formation may occur under tensile stresses in the region where unloading waves interact. When subjected to pulse loading with amplitudes on the order of the Hugoniot Elastic Limit, ZrB_2-ZrO_2, ZrB_2-B_4C ceramic composites can accumulate damage while macroscopic strength is preserved.

Fig.4. shows damage pattern behind the front of the elastic precursor with amplitude of 6GPa, behind the front of shock wave with amplitude of 10 GPa at 6 10^{-10} s. Figs. 4 (a) and (b) shows the pattern of local damages behind the shock wave front in composites ZrB_2-ZrO_2 (a), ZrB_2-B_4C (b) with uniform distributed inclusions at 6 10^{-10} s.

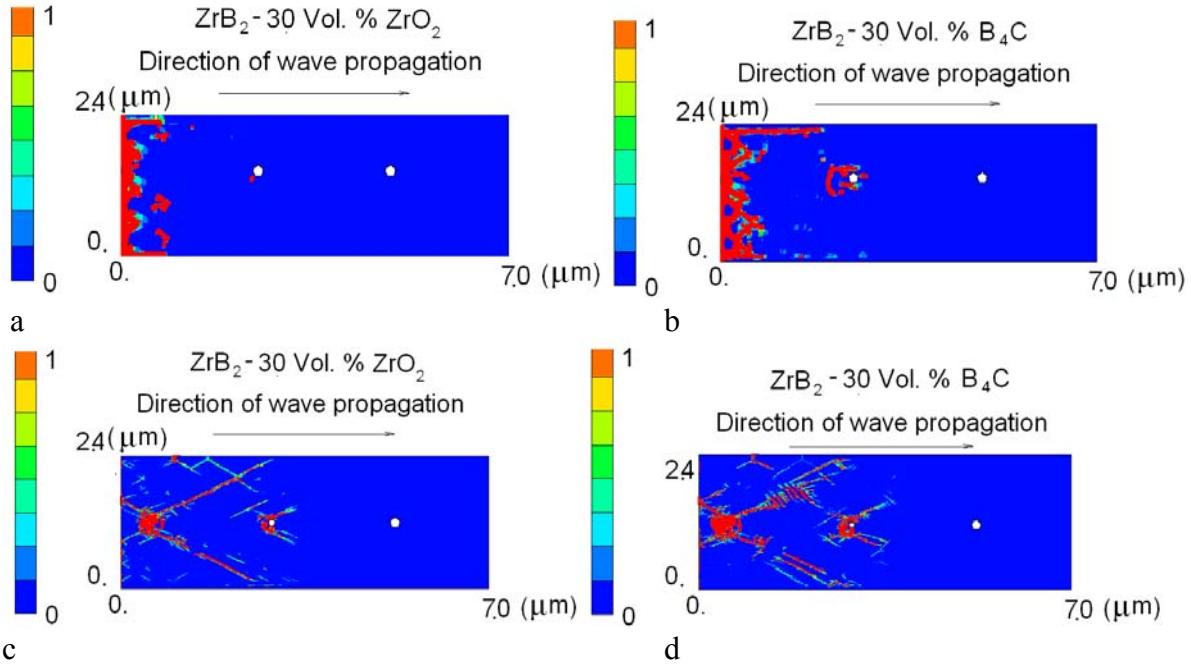

Fig.4. Numerical simulation of damage in ZrB_2- 30 Vol. % ZrO_2 and ZrB_2- 30 Vol. % B_4C.

Fig. 4c,d shows the distribution of local damages behind the shock wave front in composites ZrB_2-ZrO_2 (a), ZrB_2-B_4C (b) with clusters of inclusions (See Fig.2(b)). It's found that clusters of strengthening inclusions cause a decrease in the macro-scale fracture stress threshold.

Results of simulation show that damage of nano-composites near voids can be formed under stress pulse amplitude less than the Hugoniot elastic limit of matrix.

Self-organization process of micro-damages and occurrence of mesoscale shear band were observed in the ceramic nano-composite under compression at high strain rates (See Fig. 4(c,d)).

These results are in agreement with data obtained in [20, 21].

Tensile stress gradients occurring in the region, where unloading waves interact, are most dangerous for nanocomposites. In the absence of coarse strengthening elements (fibers, particles), which can play a role of barrier that blocks micro-crack opening and propagation, the spall strength of nanocomposites depends mainly on relative volume and size of voids.

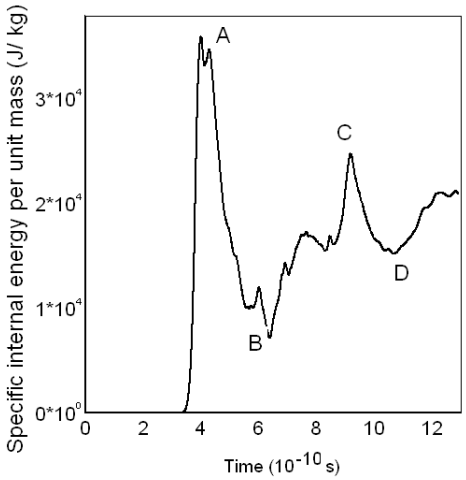

Fig.5. Specific internal energy per unit mass of ZrB_2- 30 Vol. % B_4C

Fig.5 shows the drops in local specific internal energy of ZrB_2- 30 Vol. % B_4C nanocomposite in the point at boundary of the first and second RVE (See Fig.2).

Obtained numerical results confirm the findings [22] that damage mechanisms of different characteristic duration take place in nanostructured materials. Fracture of ceramic nanocomposites under pulse and shock-wave loadings is provided by fast processes of intercrystalline brittle fracture (curve part AB) and relatively slow processes of ductile fracture via growth and coalescence of microvoids and opened microcracks (curve part BCD).

In particular, brittle behavior is realized effectively under high strain rates. Ductile fracture is realized via microvoids coalescence mechanism. Thereby fracture of ceramic nanocomposites under pulse loadings has a quasi-brittle behavior.

4 CONCLUSIONS

Multi-scale computer simulation approach was applied to research of mechanisms of failure in ceramic nanocomposites under dynamic loading. Damage nucleation and accumulation in quasi brittle ceramics nanocomposites were simulated under impact loadings.

The probability of fracture was estimated for $ZrO_2 - ZrB_2$, and $ZrB_2 - B_4C$ nanocomposites under pulse loadings of microsecond duration.

The computational models of a structured representative volume (RVE) of ceramic nanocomposites were developed using the data of structure researches at meso-, micro -, and nanoscale levels.

The critical fracture stress on meso-scale level depends not only on relative volumes of voids and inclusions, but also on the parameters of inclusions clusters.

Damage of $ZrO_2 - ZrB_2$, and $ZrB_2 - B_4C$ nano-composites can be formed under stress pulse amplitude of less than the Hugoniot elastic limit of matrix. These damages caused the changes of the spall strength of nano-composites.

The Hugoniot elastic limit of ceramic nanocomposites decreases with increasing volume concentration of nano-void clusters.

The spall stress of ceramic nanocomposites depends on relative volumes and sizes of voids and inclusions.

Self-organization process of micro-damages and occurrence of mesoscale shear band were observed in the ceramic nano-composite under compression at high strain rates.

ACKNOWLEDGMENTS

This work is supported by Ministry of Sciences and Education of Russian Federation (State task №2014/223, project № 1943), also by the Grant from the President of the Russian Federation, and partially RFBR (project 08-08-12055). The authors are grateful for the support of this research.

REFERENCES

[1] Bakshi, S. D., Basu, B. , and Mishra S. K. Microstructure and mechanical properties of sinter-HIPed ZrO_2–ZrB_2 composites. *Composites*: *Part A.* (2006) **37**: 2128–2135.

[2]. Huang, S.G., Vanmeensel, K., Vleugels, J. Powder synthesis and densification of ultrafine B_4C-ZrB_2 composite by pulsed electrical current sintering. *J. of the European Ceram. Soc.* (2014) **34**: 1923-1933.

[3] Petrov, Y.V., Karihalo, B.L., Bratov, V.V., and Bragov, A.M. Multi-scale dynamic fracture model for quasi-brittle materials *Int. J. of Engng Sci.* (2012) **61**: 3–9.

[4] Skripnyak, E. G., Skripnyak, and V.A., Skripnyak, V. V. Fracture of nanoceramics with porous structure at shock wave loadings. *Shock Compression of Condensed Matter. AIP Conf. Proc*. 2012. **1426**: 965 -970.; doi: 10.1063/1.3686485.

[5] Liu, Q., Han, W., and Hu P. Microstructure and mechanical properties of ZrB_2–SiC nanocomposite ceramic. *Scripta Materialia*. (2009) **61**: 690-692.

[6] Teng, Yu., Sun, Zh., Zhang, K., Lu, W. Microstructure and mechanical properties of high-pressure sintered Al_2O_3/SiC nanocomposites. *J. of Alloys and Comp.* 2013. **578**: 67-71.

[7] Zavattieri, P.D., Raghuram, P.V., and Espinosa, H.D. A computational model of ceramic microstructures subjected to multi-axial dynamic loading. *J Mech Phys. Solids.* (2001).**49**: 27–68.

[8] Zhang, W.X., Wang,T.J., Chen X. Effect of surface/interface stress on the plastic deformation of nanoporous materials and nanocomposites *Int. J. of Plasticity*. (2010) **26**: 957-975.

[9] Tomar, V. Analyses of the role of grain boundaries in mesoscale dynamic fracture resistance of SiC–Si_3N_4 intergranular nanocomposites *Engng Fract. Mech.* (2008) **75**: 4501-4512.

[10] Quaresimin, M., Salviato, M., and Zappalorto, M. Strategies for the assessment of nanocomposite mechanical properties *Composites: Part B.* (2012) **43**: 2290–2297.

[11] Mantena, P.R., Al-Ostaz, A., and Cheng, A.H.D. Dynamic response and simulations of nanoparticle-enhanced composites *Composites Sci. and Tech.* (2009) **69**: 772-779.

[12] Hasheminejad, S. M., and Avazmohammadi, R. Size-dependent effective dynamic properties of unidirectional nanocomposites with interface energy effects. *Composites*

Sci. and Tech. (2009) **69**: 2538-2546.
[13] Johnson, G. R. , and Holmquist, T. J. Response of boron carbide subject to large strains, high strain rates and high pressures. *J. Appl. Phys.* 1999 **85**: 8060–8073.
[14] Parshikov, A.N., Medin, S.A., Loukashenko, I.I., and Milekhin, V.A. Improvements in SPH Method by means of interparticle contact algorithm and analysis of perforation tests at moderate projectile velocities. *Int. J. Impact Eng.* (2000) **24**: 779-796.
[15] Parshikov A.N., Medin S.A. Smoothed particle hydrodynamics using interparticle interparticle contact algorithms. *J. Comp. Phys.* (2002) **180**: 358-382.
[16] Gust, W. H. , and Royce, E. B. Dynamic yield strengths of B4C, BeO, and Al_2O_3 ceramics. *J. Appl. Phys.* (1971) **42**: 276–295.
[17] Gust, W. H., Holt, A. C. , and Royce, E. B. Dynamic yield, compressional, and elastic parameters for several lightweight intermetallic compounds. *J. Appl. Phys.* (1973)**44**: 550–560.
[18] Batsanov, S.S. *Effects of explosions on materials: Modification and synthesis under high-pressure shock compression.* Springer, (1994).
[19] *Physical values. Handbook*. Eds. By Babichev, A.P., Bratkovskii, A.M. et al. Moscow. Energoatomizdat. (1991).
[20] Levy, S., and Molinari J.F. Dynamic fragmentation of ceramics, signature of defects and scaling of fragment sizes. *J. of the Mech. and Phys. of Solids* (2010) 58: 12–26.
[21] Skripnyak E.G., Skripnyak, V.V., Vaganova, I.K., and Skripnyak,V.A. Fracture of Ceramic Materials under Dynamic Loadings. *Proc. 19th European Conf. on Fracture (ECF19) Kazan, Russia.* (2012) 639.
[22] Ovid'ko, I.A. Cracks nucleation in nanomaterials at high-speed and quasistatic modes deformations materials. *Physics and Mechanics* (2011) **12:** 76-101.